Providence, RI
NOISE-CON 2016
2016 June 13-15

Numerical study of an in-situ technique for measuring surface impedance and reflection coefficient of a locally reacting material with pressure-velocity probes

Graciano Carrillo Pousa
Daniel Fernández Comesaña
David Pérez Cabo
Microflown Technologies
Tivolilaan 205, Arnhem
6824 BV
Netherlands
info@microflown.com

Andrés Prieto
Department of Mathematics
Faculty of Computer Science
University of A Coruña
Campus Elviña s/n
15071 A Coruña
Spain

ABSTRACT

The characterization of the acoustic sound pressure and velocity field on the surface of absorbing materials plays a key role for the computation of their surface impedance and absorption coefficients. In this work, a technique based on the equivalent source method (ESM) is used to estimate the pressure and velocity field in order to compute the surface impedance and reflection coefficient of a locally reacting surface. The assessed in-situ technique only requires measuring on a single layer with an array of pressure-velocity (*p*-*u*) probes. A numerical simulation study is performed to compare the estimated values with those obtained using a double layer of pressure sensors. Results show a significant improvement in the lower frequency range in terms of both reconstruction accuracy and robustness against noise.

1 INTRODUCTION

The in-situ characterization of acoustic impedance and reflection coefficient of materials is of considerable interest for a wide range of applications. In recent years, there has been an increasing amount of literature on novel in-situ methods which can be categorized in two major groups. On the one hand, several methods rely upon assumptions about the excitation sound source and the reflected sound field[1,2,3], such as planar, mirror model with planar reflection or spherical wave model. Such techniques often suffer from limitations when the assumptions are not satisfied in a real environment. On the other hand, sound field reconstruction techniques can also be applied without prior information about the sound field. One of the most commons methods was introduced by Tamura[4] based on the spatial Fourier Transform of sound pressure measurements at two parallel planes. With a similar configuration, an in-situ technique based on the Equivalent Source Method (ESM) was presented by Zhang et al.[5] The ESM method has significant advantages over Tamura technique, such as a smaller measurement aperture and more accurate results. In contrast, it is currently limited to locally reactive materials because the ESM-based method is not able to compute the reflection coefficients at several angles of incidence[5]. In addition, a novel technique has recently been proposed for oblique incidence based on statistically optimized near-field acoustic holography (SONAH) also using several layers of sound pressure microphones[6].

After the introduction of particle velocity transducers, sound field reconstruction techniques using a single-layer of *p-u* probes have also been developed[7,8]. Although ESM-based methods have already been used in combination with sound pressure microphones and particle velocity sensors, a comparison of the performance achieved when determining surface impedance and reflection coefficient has not yet been undertaken.

In this paper, ESM-based methods are studied for the determination of the surface impedance and the reflection coefficient of locally reactive surfaces. Results obtained with a single layer of sound pressure microphones and particle velocity sensors (*p-u*) are compared with a double layer configuration of sound pressure microphones. In the following sections the theory of the ESM-based methods is described for both single layer and two layers case. A numerical study is presented, including results and a discussion about the performance of both methods.

2 THEORY: MEASUREMENT TECHNIQUES BASED ON ESM

ESM relies on modeling the sound field as the superposition of waves generated by a set of point sources. This key concept allows for splitting the contributions of different sources and it can be used for separating the incoming and reflected sound field. This idea is also suitable for the characterization of the surface impedance and the reflection coefficient of multiple materials.

The evaluated techniques use sound pressure or/and particle-velocity measured in one or two planes in the near-field of the tested sample, while the sound field is excited by a sound source at normal incidence. Inverse techniques are applied to estimate the strength of the sound source and its image source, in such a way that the sound field on the surface can be recovered. As a result, the surface impedance and reflection coefficient can then be computed. In the following sections a general formulation of ESM for single layer of pressure-velocity probes and a double layer of pressure microphones is described. A sketch of both approaches is shown in Fig. 1.

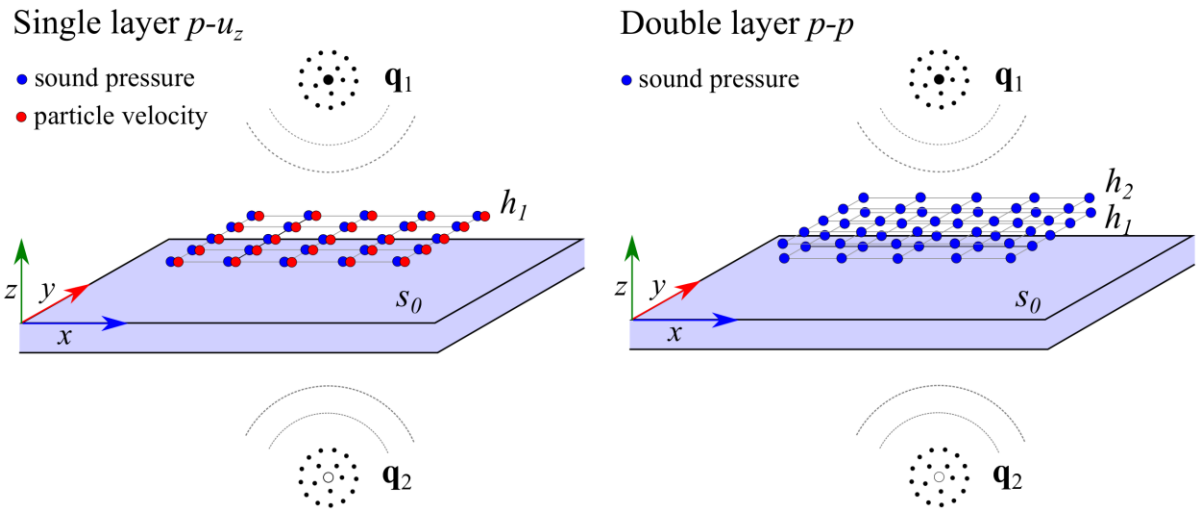

Figure 1: *Sketch of the Equivalent Source Method configuration for single layer p-u (left) and double layer p-p (right).*

2.1 Single layer pressure-velocity (*p-u*)

Sound pressure and particle velocity can be expressed as the result of the superposition of the sound field created by multiple point sources. Considering the special case of having a sound source over a certain surface, the resulting sound field at the plane $z = h_1$ can be modeled as the

combination of a set of equivalent sound sources $\mathbf{q}_1$ and its set of image sources $\mathbf{q}_2$ as shown in Fig. 1. Hence,

$$\begin{bmatrix}\mathbf{p}_{h_1}\\ \mathbf{u}_{h_1}\end{bmatrix} = \begin{bmatrix} j\omega\rho\mathbf{G}_{q_1h_1} & j\omega\rho\mathbf{G}_{q_2h_1} \\ -\mathbf{G}^u_{q_1h_1} & -\mathbf{G}^u_{q_2h_1}\end{bmatrix}\begin{bmatrix}\mathbf{q}_1\\ \mathbf{q}_2\end{bmatrix}, \tag{1}$$

where the column vectors $\mathbf{p}_{h_1}$ and $\mathbf{u}_{h_1}$ are the pressure and the *z*-component of particle velocity located on the plane $z = h_1$, the vectors $\mathbf{q}_1$ and $\mathbf{q}_2$ are the equivalent source strengths that model the sound source and its image source, $\mathbf{G}_{q_ih_j}$ and $\mathbf{G}^u_{q_ih_j}$ are transfer functions that relate the propagation from the sources $\mathbf{q}_i$ to the plane $z = h_j$, ω is the angular frequency and ρ is the air density. These transfer functions are defined as the Green's function in free-space and its derivative in the normal direction (to the measurement plane $z = h_1$), thus

$$\mathrm{G}(\mathbf{r}, \mathbf{r}_i) = e^{-jk|\mathbf{r}-\mathbf{r}_i|}, \tag{2}$$

$$\mathrm{G}^u(\mathbf{r}, \mathbf{r}_i) = \frac{\partial}{\partial z}\mathrm{G}(\mathbf{r}, \mathbf{r}_i), \tag{3}$$

where k is the wavenumber, $\mathbf{r}_i$ denotes the source position and $\mathbf{r}$ is the location where the sound field is computed. The equivalent source strength vectors $\mathbf{q}_1$ and $\mathbf{q}_2$ can be estimated by solving an inversion problem in Equation (1) using a weighted least squares solution as proposed in[9,10],

$$\mathbf{q} = (\mathbf{WG})^{+}\mathbf{Wb}, \tag{4}$$

$$\mathbf{W} = \begin{pmatrix} ||\mathbf{p}_h|| & 0 \\ 0 & ||\mathbf{u}_h|| \end{pmatrix}^{-\mathbf{1}}, \tag{5}$$

where $\mathbf{q}$ is composed by the vectors of sources $\mathbf{q}_1$ and $\mathbf{q}_2$, $\mathbf{G}$ is the transfer matrix, $\mathbf{b}$ is a vector that contains the measured sound pressure $\mathbf{p}_h$ and the particle velocity $\mathbf{u}_h$, and $\mathbf{W}$ is a weighting diagonal matrix. The superscript $^+$ refers to the Tikhonov regularized pseudo-inverse:

$$(\mathbf{WG})^{+} = ([\mathbf{WG}^{\mathrm{H}}]\mathbf{WG} + \lambda\mathbf{I})^{-1}[\mathbf{WG}^{\mathrm{H}}], \tag{6}$$

where λ is the regularization parameter and $\mathbf{G}^{\mathrm{H}}$ is the Hermitian transpose of matrix $\mathbf{G}$. The need of a weighting matrix $\mathbf{W}$ arises from the differences in magnitude between the sound pressure and the particle velocity by approximately the characteristic acoustic impedance. The application of a weighting factor avoids the residual of the minimization process to be dominated by the pressure error.

The sound pressure and the particle velocity on the material surface $z = s_0$ can be reconstructed via the Green's functions shown in Equations (2)-(3) to account for the sound propagation from the estimated equivalent sources $\mathbf{q}_1$ and $\mathbf{q}_2$. In this manner, the pressure and the *z*-component of the particle velocity are given by

$$\mathbf{p}_{s_0} = j\omega\rho\left(\mathbf{G}_{q_1s_0}\mathbf{q}_1 + \mathbf{G}_{q_2s_0}\mathbf{q}_2\right), \tag{7}$$

$$\mathbf{u}_{s_0} = -\left(\mathbf{G}^u_{q_1s_0}\mathbf{q}_1 + \mathbf{G}^u_{q_2s_0}\mathbf{q}_2\right). \tag{8}$$

It is possible to compute the surface impedance Z_{s_0} and reflection coefficient $R_{s_0}(\theta)$ by using the estimation of the pressure and velocity fields at *N* points on the surface $z = s_0$, given in Equations (7)-(8). Consequently, given the point values of pressure and velocity fields, $p^{(n)}_{s_0}$ and $u^{(n)}_{s_0}$, averaged estimates can be obtained by applying the following relationships:

$$Z_{s_0} = \frac{1}{N}\sum_{n=1}^{N}\frac{p_{s_0}^{(n)}}{u_{s_0}^{(n)}}, \tag{9}$$

$$R_{s_0}(\theta) = \frac{Z_{s_0}\cos\theta - Z_0}{Z_{s_0}\cos\theta + Z_0}, \tag{10}$$

where Z_0 is the characteristic acoustic impedance ρc. Note that the expression of the reflection coefficient for different angles in Equation (10) is valid under the assumption of locally reactive surfaces, which holds for the present work.

2.2 Double layer pressure-pressure (*p-p*)

As shown in[5,11] the equivalent sources method can also be applied based on the measurement of sound pressure on the two planes $z = h_1$ and $z = h_2$,

$$\begin{bmatrix}\mathbf{p}_{h_1}\\ \mathbf{p}_{h_2}\end{bmatrix} = j\omega\rho\begin{bmatrix}\mathbf{G}_{q_1h_1} & \mathbf{G}_{q_2h_1}\\ \mathbf{G}_{q_1h_2} & \mathbf{G}_{q_2h_2}\end{bmatrix}\begin{bmatrix}\mathbf{q}_1\\ \mathbf{q}_2\end{bmatrix}, \tag{11}$$

where the vectors $\mathbf{p}_{h_1}$ and $\mathbf{p}_{h_2}$ correspond to measurements of the sound pressure on the planes $z = h_1$ and $z = h_2$; the transfer functions $\mathbf{G}_{q_ih_j}$ are given by Equation (2) which models the sound propagation from the sources $\mathbf{q}_i$ to the plane h_j.

To solve the inversion problem, a regularized inversion approach analogous to the one presented in Section 2.1 is used. In this case there is no need to apply any weighting procedure. Based on the estimated equivalent source strength vectors $\mathbf{q}_1$ and $\mathbf{q}_2$, the sound pressure and the particle velocity on the surface $z = s_0$ are obtained by using Equations (7)-(8). The surface impedance and the reflection coefficient can then be estimated by employing Equations (9)-(10).

3 NUMERICAL STUDY

A numerical investigation has been conducted to study the performance of the ESM-based methods described in the previous sections. The sound field produced by a sound source over a locally reactive surface was simulated following the model proposed by Di and Gilbert[12]. The sound pressure above an infinite plane with given impedance is derived assuming a locally reactive surface. The sound pressure and particle velocity generated by a time-harmonic sound source of volume velocity Q at a position $\mathbf{r}$ are defined as,

$$p(\mathbf{r}) = \frac{j\omega\rho Q}{4\pi}\left(\frac{e^{-jk|\mathbf{r}-\mathbf{r}_1|}}{|\mathbf{r}-\mathbf{r}_1|} + \frac{e^{-jk|\mathbf{r}-\mathbf{r}_2|}}{|\mathbf{r}-\mathbf{r}_2|} - 2k\beta\int_0^\infty e^{k\beta q}\frac{e^{-jk\sqrt{d_1^2+(r_{1z}+r_z-jq)^2}}}{\sqrt{d_1^2+(r_{1z}+r_z-jq)^2}}dq\right), \tag{12}$$

$$u_z(\mathbf{r}) = -\frac{1}{j\omega\rho}\frac{\partial}{\partial z}p(\mathbf{r}), \tag{13}$$

where $\mathbf{r}_1$ and $\mathbf{r}_2$ are the locations of the sound source and its image source, r_z and r_{1z} are the heights of the measurement point and the sound source with respect to the material surface, d_1 is the horizontal distance between the sound source and $\mathbf{r}$, and $\beta = Z_0/Z_{s_0}$ is the normalized surface acoustic admittance at normal incidence.

The absorbing surface material under test is supposed to be locally reacting. Thus, the input impedance related to the acoustic behavior of a porous layer is assumed independent of the angle of incidence of the sound waves. Under this assumption, the ESM method could be applied and the reflection coefficient could also be computed for several angles of incidence. Without loss of

generality, the model for the porous material is assumed to be of the type Delany and Bazley[13]. The surface impedance with a given flow resistivity ϱ (in Nms^{-4}) at a frequency f is given by

$$Z_s(f) = Z_0\left[1 + 9.08\left(\frac{10^3 f}{\varrho}\right)^{-0.75} - j11.9\left(\frac{10^3 f}{\varrho}\right)^{-0.73}\right]. \quad (14)$$

A sound source was placed 0.1 m above the material while a uniform line array was located at certain distance above the surface along the *x*-axis. For the single layer *p-u* configuration the array was located at $z = 0.01$ m, while the double layer *p-p* sensor array was at $z = 0.01$ m and $z = 0.03$ m. The sound field was measured at 21 equally spaced points in the interval $[-0.01,0.01]$ m at the x-axis. Despite the axial symmetry of the problem, sensors were placed at both sides of the x-axis in order to account for uncorrelated noise between transducers. The equivalent sources were located in two circles with a radius of 0.01 m around the sound source and its image source, consisting of 12 elements at each location. A sketch of the problem addressed is illustrated in Fig. 2.

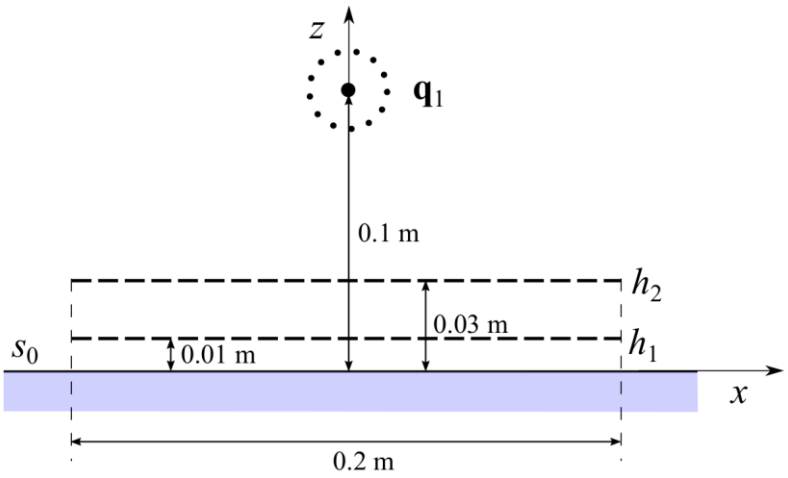

Figure 2: Sketch of the numerical simulation configuration.

The noise added to the simulated data was assumed white isotropic Gaussian noise of equal variance for all transducers with a fixed SNR of 30 dB. All results presented were obtained using a Monte Carlo simulation over 100 runs.

Results are assessed by evaluating the reconstruction error with respect to the reference values. The relative error $E\{\gamma_{\text{est}}\}$ of an arbitrary estimation γ_{est} is calculated with respect to the reference γ_{ref} as follows,

$$E\{\gamma_{\text{est}}\} = 20\log_{10}\left(\frac{\left|\left|\gamma_{\text{est}} - \gamma_{\text{ref}}\right|\right|_2}{\left|\left|\gamma_{\text{ref}}\right|\right|_2}\right). \quad (15)$$

In the following sections a comparison between methods, single layer *p-u* and double layer *p-p* is presented. Firstly, the estimated surface impedance and reflection coefficient are evaluated. Secondly, the influence of different SNRs on the reconstruction results is studied.

4 RESULTS AND DISCUSSION

A numerical investigation has been performed with two main objectives: to study the performance of ESM-based methods with the two different configurations and to assess the impact of different SNR conditions on the reconstruction error across frequency.

4.1 Surface Impedance and Reflection Coefficient for fixed SNR

Results of normalized surface impedance estimations are shown in Fig 3. The reconstruction error indicates that the double layer *p-p* configuration achieves a good performance for frequencies above 800-1000 Hz, where the relative reconstruction error is below -20 dB (i.e. 10% error). In contrast, the *p-u* single layer shows a good performance also for lower frequencies, even at 300 Hz.

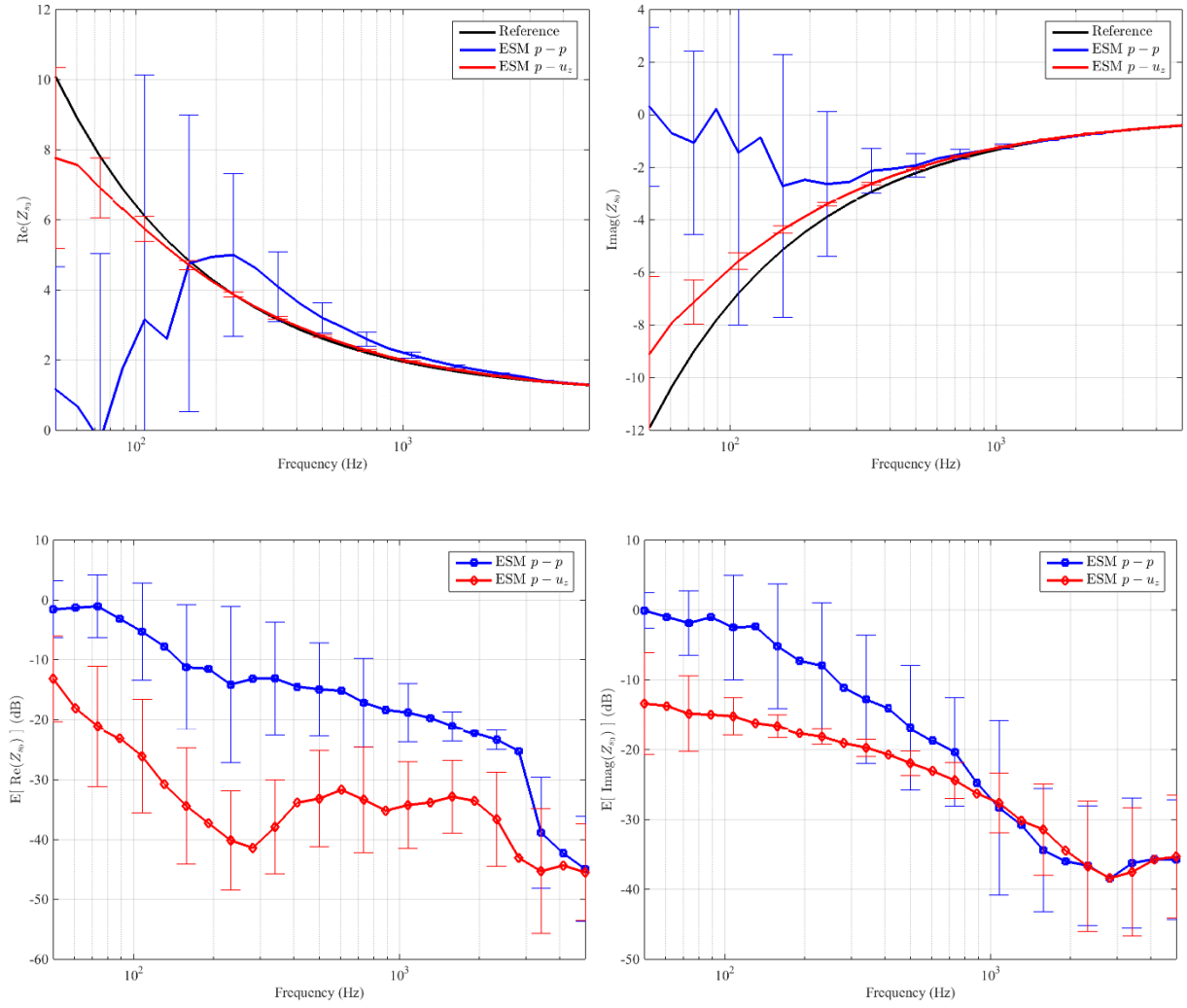

Figure 3: Normalized complex surface impedance: real part (top left), imaginary part (top right), relative error of real part estimation (bottom left) and relative error of the imaginary part estimation (bottom right). A confident interval of 95% is displayed with the same colors as the method used.

Results obtained for the reflection coefficient R_{s_0} are presented in Fig. 4. As shown, the *p-p* double layer configuration has significant performance differences in the reconstruction of the real and the imaginary part. The reconstruction error of the imaginary part is acceptable above 1500 Hz, while the real part is valid from 200 Hz. On the other hand, the single layer *p-u* array yields accurate results from 50 Hz for both real and imaginary part of the reflection coefficient.

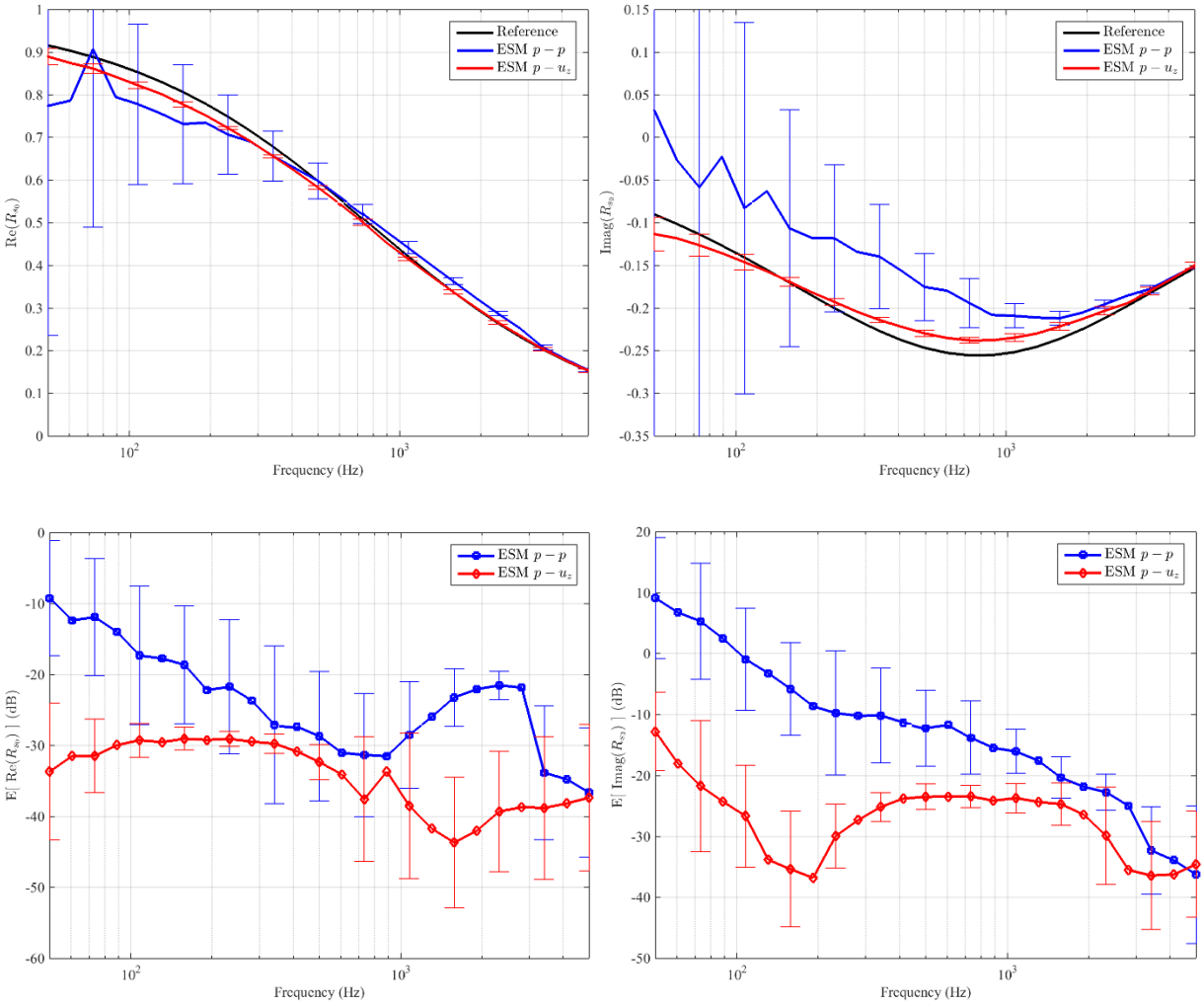

Figure 4: Normalized complex reflection coefficient: real part (top left), imaginary part (top right), relative error of real part estimation (bottom left) and relative error of the imaginary part estimation (bottom right). A confident interval of 95% is displayed with the same colors as the method used.

Interestingly, reconstruction results of the reflection coefficient using the *p-u* configuration are more consistent and less sensitive to noise than the ones obtained for the surface impedance. Furthermore, results achieved with the *p-p* configuration have a greater variance across the Monte Carlo runs. In conclusion, the reconstruction error and the variance of the results suggest that the single layer *p-u* configuration is generally more robust and accurate than the double layer *p-p* array, especially in the low frequency range.

4.2 Surface Impedance reconstruction error for variable SNR

The SNR plays a key role in the performance and robustness of ESM methods. Previous results suggest that both tested configurations are affected by noise in a different manner. In order to gain a better understanding about the influence of noise on the reconstructions, an additional Monte Carlo simulation has been undertaken. Relative reconstruction errors obtained with both configurations are presented in Fig. 5 for different levels of SNR, using light colors to indicate large errors.

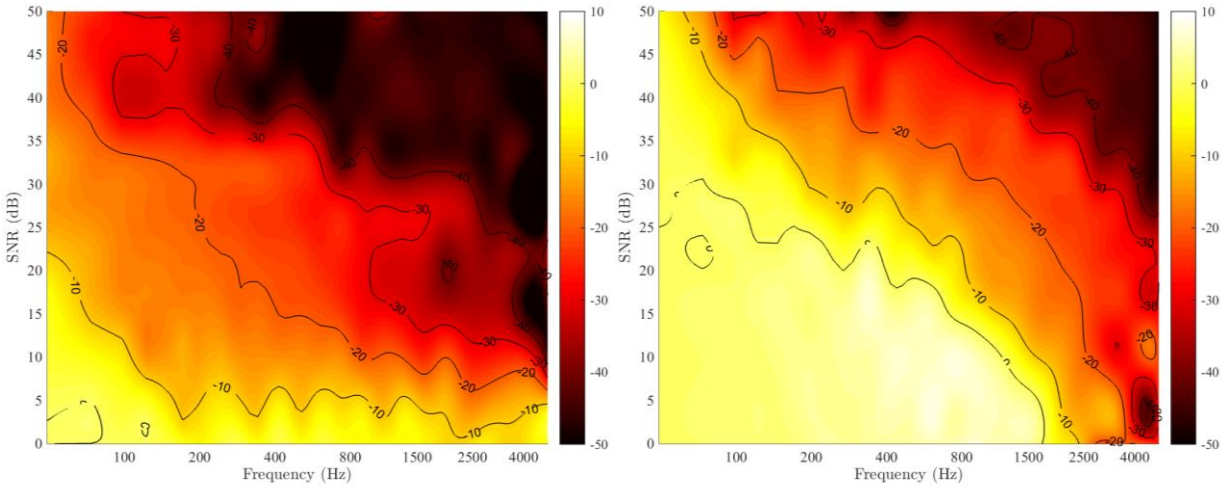

Figure 5: Reconstruction error of the surface impedance for variable SNR and frequencies with two different sensor configurations: single layer *p-u* (left) and double layer *p-p* (left).

As shown in Fig 5, the *p-u* method significantly outperforms the *p-p* configuration, especially in the low frequency range (< 1000 Hz). A possible explanation for this effect could be differences between interference patterns in terms of sound pressure and particle velocity. The ability to acquire the two quantities at the same plane seems key for avoiding large estimation errors when the wavelength is large.

5 CONCLUSION

The acoustic properties of a complex surface have been calculated using both a single-layer of *p-u* probes and a double layer of sound pressure microphones in combination with ESM. A numerical comparison of these configurations has been conducted assessing the impact of SNR on the results at different frequencies. It has been shown that both configurations yield good results (reconstruction error lower than 10%) at high frequencies, above 800 Hz for the surface impedance and 1500 Hz for the reflection coefficient. However, single layer *p-u* has a significantly better performance in the low frequency range, for wavelengths that are much larger than the distance to the surface or spacing between layers of the *p-p* configuration. In addition, the single layer *p-u* is also most robust against noise, achieving accurate results with relatively low levels of SNR.

6 REFERENCES

1. E. Brandão, A. Lenzi, and S. Paul. "A Review of the In Situ Impedance and Sound Absorption Measurement Techniques". *Acta Acustica united with Acustica* 101, no. 3, (2015): 443-463.
2. J. D. Alvarez and F. Jacobsen, "An iterative method for determining the surface impedance of acoustic materials in situ", *Proceedings of Inter-Noise* (2008).
3. C. Nocke, V. Mellert, T. Waters-Fuller, K. Attenborough, and K. M. Li. "Impedance deduction from broad-band, point-source measurements at grazing incidence", *Acta Acustica United with Acustica* 83, no. 6 (1997): 1085-1090.
4. M. Tamura, "Spatial Fourier transform method of measuring reflection coefficients at oblique incidence. I: Theory and numerical examples", *Journal of Sound and Vibration* 152, (1990): 5-88.
5. Y.-B. Zhang, W.-L. Lin and C.-X. Bi, "A technique based on the equivalent source method for measuring the surface impedance and reflection coefficient of a locally reacting material", *Proceedings of Inter-Noise* (2014).
6. M. Ottink, J. Brunskog, C. H. Jeong, E. Fernandez-Grande, P. Trojgaard, and E. Tiana-Roig, "In situ measurements of the oblique incidence sound absorption coefficient for finite sized absorbers". *The Journal of the Acoustical Society of America* 139, no. 1, (2016): 41-52.

7. F. Jacobsen, V. Jaud, "Statistically optimized near field acoustic holography using an array of pressure-velocity probes". *The Journal of the Acoustical Society of America*, 121, no. 3 (2007): 1550-1558.
8. E. Fernandez-Grande, Near-field acoustic holography with sound pressure and particle velocity measurements. PhD Thesis, Technical University of Denmark, (2012).
9. P. C. Hansen, "Analysis of discrete ill-posed problems by means of the L-curve", *SIAM* Review 34 (1992): 561-580.
10. E. Fernandez-Grande, F. Jacobsen, and Q. Leclere. "Sound field separation with sound pressure and particle velocity measurements." *The Journal of the Acoustical Society of America* 132, no. 6 (2012): 3818-3825.
11. Y.-B. Zhang, F. Jacobsen, C.-X. Bi, and X.-Z. Chen. "Near field acoustic holography based on the equivalent source method and pressure-velocity transducers." *The Journal of the Acoustical Society of America* 126, no. 3 (2009): 1257-1263.
12. X. Di and K.E. Gilbert. "An exact Laplace transform formulation for a point source above a ground surface." *The Journal of the Acoustical Society of America* 93, no. 2 (1993): 714-720.
13. M. E. Delany and E. N. Bazley. "Acoustical properties of fibrous absorbent materials." *Applied acoustics* 3, no. 2 (1970): 105-116.